

CLAP: Unsupervised 3D Representation Learning for Fusion 3D Perception via Curvature Sampling and Prototype Learning

Runjian Chen¹ Hang Zhang² Avinash Ravichandran² Hyoungseob Park³ Wenqi Shao⁴
Alex Wong^{3*} Ping Luo^{1*}

¹The University of Hong Kong ²Cruise ³Yale University ⁴Shanghai AI Laboratory
 {rjchen, pluo}@cs.hku.hk alex.wong@yale.edu

Abstract

*Unsupervised 3D representation learning reduces the burden of labeling multimodal 3D data for fusion perception tasks. Among different pre-training paradigms, differentiable-rendering-based methods have shown most promise. However, existing works separately conduct pre-training for each modalities due to computational costs of processing large point clouds with images. As such, mutual benefit of high-level semantics (from image) and 3D structure (from point cloud) has not been exploited. To address this gap, we propose a joint unsupervised differentiable-rendering-based pre-training method for images and point clouds, termed CLAP, short for **C**urvature samp**L**ing and **leA**rnable **P**rototype. Specifically, our method overcomes the computational hurdle by Curvature Sampling to select the more informative points/pixels for pre-training. To uncover the performance benefits brought by their complementarity, we propose to use learnable prototypes to represent parts of the 3D scenes in a common feature space and an Expectation-Maximization training scheme to associate embeddings of each modality to prototypes. We further propose a swapping prediction loss that explores their interplay through prototypes along with a Gram Matrix Regularization term to maintain training stability. Experiments on NuScenes and Waymo datasets show that CLAP achieves up to 100% more performance gain as compared to previous SOTA pre-training methods. Codes and models will be released.*

1. Introduction

3D perception facilitates spatial applications such as autonomous driving. The autonomous system, on which these applications are deployed, are typically equipped with multiple sensors including visual ones like cameras that pro-

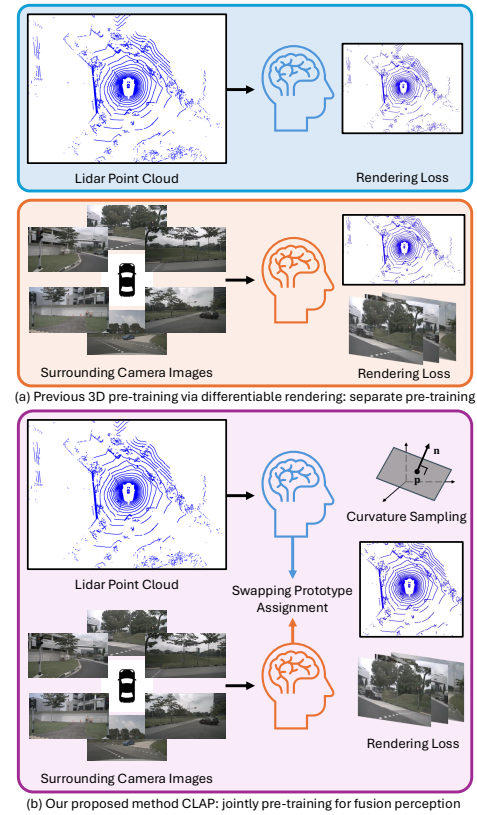


Figure 1. Unlike previous SOTA unsupervised 3D representation learning method UniPAD [58] that separately pre-train LiDAR and camera encoders with differential rendering (a), our proposed method CLAP conducts joint pre-training for fusion perception.

duce RGB images, and range sensors like LiDAR (Light-Detection-And-Ranging) that generate point clouds. Fusion of these two modalities [8, 21, 22, 25, 26, 30, 32] have generally improved over use of a single modality, e.g., camera [7, 11, 20, 43, 50, 60] or LiDAR [1, 12, 39, 42, 55, 59] separately, in 3D perception performance.

However, training multimodal 3D perception models is

*Corresponding authors.

expensive as labeling in 3D space is notoriously time-and-energy-consuming. Unsupervised 3D representation learning, which pre-trains backbones without any label and fine-tuned the pre-trained weight for downstream performance improvement, has shown the potential to alleviate the labeling burden in 3D perception. Amongst the many unsupervised 3D pre-training methods [6, 18, 19, 24, 53, 57, 58, 62], use of mask auto-encoding (reconstruction) and differentiable rendering has emerged as the most performant. However, encoding and processing high-dimensional multi-modal data (images and point clouds) is computationally expensive: If one were to pre-train using all points and pixels within the point cloud and image, respectively, even the most advanced GPU to date (H100) is only able to hold a batch size of 1. Therefore, existing methods, e.g., UniPad [58], has conventionally pre-trained each modality separately. While the two modalities are complementary (semantics from image, and structure from point clouds), current methods are unable to exploit their mutual benefits during pre-training.

To address this pain point, we propose a joint unsupervised pre-training method of image and point cloud modalities based on differentiable rendering. Our method, CLAP, short for Curvature sampLing and leArnable Prototype, addresses the primary computational challenge by a curvature sampling strategy, which comes from the observation that there exists redundancy in information when sampling multiple points on the same flat surface. This is enabled by estimating the curvature of each point in the 3D space by taking second order derivative of the SDF (signed distance field) function. This allows us to identify points at which large change in the surface occurs. Through calibration, we can obtain the corresponding pixel within the image, around which we sample assuming the coordinates are normally distributed. This sampling strategy captures variations in the point cloud and in turn provide more informative points than the conventional sampling strategy in [58].

As our curvature sampling strategy has reduced the computational burden to allow both modalities to be simultaneously processed, we propose to model the interplay between image and point cloud modalities through a set of learnable prototypes, which represents parts of the 3D scene and enables a common feature space to bridge the two modalities. These prototypes are trained via an Expectation-Maximization (EM) algorithm that maximizes similarity between embeddings for each modality and the set of prototypes. Furthermore, we propose to use the swapping prediction loss to explore the interaction between the two modalities. Last but not least, we utilize a Gram Matrix Regularization term to minimize similarity across prototypes, which addresses collapse of prototype when trained naively.

Our contributions are 4-folds: (1) We propose a curvature sampling strategy to identify informative points

(and pixels) for sampling, which enables the first joint differentiable-rendering-based pre-training method for fusion perception. (2) Learnable prototypes are utilized to learn a common feature space and an Expectation-Maximization approach is proposed to train the prototypes to represent parts of the 3D scene. (3) We further propose to use a swapping prediction loss for modality interplay and a Gram Matrix Regularization loss that avoids collapse of prototype learning. (4) Through extensive experiments on the popular autonomous driving datasets NuScenes [3] and Waymo [45], we demonstrate the effectiveness of CLAP. For example, CLAP achieves up to 100% more improvement than previous SOTA 3D pre-training methods and shows potential scaling property.

2. Related Work

Fusion 3D Object Detection. Light-Detection-And-Ranging (LiDAR) and camera are important sensors for autonomous driving perception. Previous works mainly focus on single-modality 3D perception. For LiDAR-based 3D object detection, there are three main streams with different embedding schemes for point clouds inputs. 1) Point-based methods [39, 41] utilize point-level embeddings for 3D object detection. 2) Voxel-based methods [1, 10, 12, 55, 56, 59] voxelize the 3D scene and use sparse convolution or transformer for embedding. 3) Point-voxel-combined methods [40, 42] utilize both embeddings from 1) and 2). For camera-based 3D perception, [7, 11, 20, 43, 50, 60] embed 2D features on image plane and project these 2D features into 3D space with estimated depth. Recently, research starts to focus on fusion 3D perception [8, 21, 22, 25, 26, 30, 32] with camera images and LiDAR point clouds as inputs. These methods mainly focus on integrating embeddings of different modalities and train both the 2D and 3D backbones in an supervised manner. As labeling in 3D space is costly, we explore unsupervised 3D representation learning for fusion 3D perception.

3D Pre-training. Annotating for 3D data is notoriously time- and energy-consuming and the emergence of unsupervised representation learning for 2D image [4, 13, 15, 16, 47, 51] provides a promising way to alleviate the annotation burden. Existing works [6, 17–19, 24, 27, 28, 36, 38, 52, 53, 57, 62] in unsupervised 3D representation learning into scene-level 3D point clouds can be divided into two contrastive-based and masked-and-reconstruction-based paradigms. Contrastive-based works [6, 17, 19, 24, 27, 28, 36, 52] propose various ways to build suitable views and conduct contrastive learning to improve the performance in downstream perception task. Inspired by [16] in image domain, [18, 53, 57, 62] propose to first mask the input point clouds and pre-train the 3D encoders with a shallow decoder for reconstructing the unmasked inputs. [23,

[44, 61] are pioneering works to introduce contrastive learning into fusion perception. They consider camera and LiDAR embeddings as different views of the scene and apply the contrastive loss between the two modalities. Inspired by the success of neural field in representing 3D scenes [33, 49] and previous attempts to introduce neural rendering to 3D pre-training for point clouds [18, 54, 62], UniPAD [58] proposes to use a differentiable-rendering decoder for masked-and-reconstruction pre-training and achieves SOTA performance for unsupervised 3D representation learning on fusion 3D perception. However, due to the high GPU memory consumption, UniPAD [58] is only able to separately pre-train the image and point cloud encoders and fails to utilize the interaction between modalities during pre-training. In this paper, we explore unsupervised joint pre-training for 2D and 3D backbones via differentiable rendering with Curvature Sampling and Prototype Learning. Previous work like SwAV [4] is related to our prototype learning part. SwAV [4] explores learnable prototypes to represent different categories in the same modality (image) and uses swapping assignment prediction loss for different views of the same image instance. On the contrary, learnable prototypes in CLAP are used to represent part of the 3D scenes and learn the interaction between modalities, which differs from the context in [4]. Thus we propose a Expectation-Maximization training scheme to maximize similarity between prototypes and 3D embeddings. Then a swapping prediction loss is used to learn the modality interaction. Furthermore, to avoid prototypes collapsing to the same vector, we propose a Gram Matrix Regularization loss.

3. Method

In this section, we introduce CLAP for joint unsupervised 3D pre-training via differentiable rendering on fusion 3D perception. As described in Fig. 2, CLAP pre-trains the image, LiDAR and fusion encoders jointly with Neural Field Rendering. In order to enable joint pre-training, Curvature Sampling is proposed as shown in (a) of Fig. 2. To further make use of both modalities, we utilize learnable prototypes to represent parts of the 3D scenes as shown in Fig. 2 (b). To optimize the learnable prototype, we train a common feature space with an Expectation-Maximization training scheme and incorporate interaction between modalities by a swapping prediction loss. Finally a Gram Matrix Regularization loss is proposed to avoid collapse in prototype learning. We first discuss the formulation and overall pipeline in Section 3.1. Then we introduce the details about neural field and differentiable rendering in Section 3.2. Finally, we describe the curvature sampling and prototype learning separately in Section 3.3 and 3.4.

3.1. Formulation and Pipeline

Notations. To begin with, we denote the input image set from N_{cam} cameras as $\mathcal{I} = \{\mathbf{I}_n \in \mathbb{R}^{H \times W \times 3}\}_{n=1}^{N_{\text{cam}}}$ and LiDAR point cloud as $\mathbf{P} \in \mathbb{R}^{N_p \times (3+d)}$. H and W are the height and width of the images and each pixel on the images has 3 values for RGB. N_p is the number of points in the LiDAR point cloud and each of them contains xyz -location and d feature channels. For example, in NuScenes [3] dataset, $d = 2$ represents the intensity and timestamp of each point and there are $N_{\text{cam}} = 6$ surrounding cameras on the autonomous vehicle. For each pair of camera image and LiDAR point cloud, we have the transformation matrix $\mathbf{T}_n \in \mathbb{R}^{3 \times 4}$ indicating the projection between the camera plane and LiDAR coordinate, where $n = 1, 2, \dots, N_{\text{cam}}$.

Encoding. The goal of unsupervised 3D representation learning for fusion perception is to pre-train the LiDAR, camera and fusion encoder in an unsupervised manner. Hence, we first voxelize and embed the raw LiDAR point cloud \mathbf{P} with LiDAR encoder $f_{\mathbf{P}}^{\text{enc}}$

$$\hat{\mathbf{P}} = f_{\mathbf{P}}^{\text{enc}}(\mathbf{P}), \quad (1)$$

where $\hat{\mathbf{P}} \in \mathbb{R}^{\hat{D} \times \hat{H} \times \hat{W} \times \hat{d}_{\text{p}}}$ is the embedded 3D features for LiDAR point cloud. \hat{D} , \hat{H} and \hat{W} are spatial resolutions of the embedded features and \hat{d}_{p} is number of feature channels after encoding. Then for camera images \mathcal{I} , $f_{\mathbf{I}}^{\text{enc}}$ encodes them with swin transformer [29] and uses $\mathcal{T} = \{\mathbf{T}_n\}_{n=1}^{N_{\text{cam}}}$ to project the 2D features to 3D space.

$$\hat{\mathbf{I}} = f_{\mathbf{I}}^{\text{enc}}(\mathcal{I}, \mathcal{T}, \mathbf{P}), \quad (2)$$

where $\hat{\mathbf{I}} \in \mathbb{R}^{\hat{D} \times \hat{H} \times \hat{W} \times \hat{d}_{\text{I}}}$ is the embedded 3D features for surrounding camera images with the similar dimensions as $\hat{\mathbf{P}}$ except for \hat{d}_{I} feature channels. The projection of 2D features to 3D space is similar to [30]: we transform LiDAR points back to image planes with \mathcal{T} and use the projected depths to project the 2D features to 3D space. With $\hat{\mathbf{P}}$ and $\hat{\mathbf{I}}$, we further concatenate them along feature dimension and apply the fusion encoder $f_{\text{fusion}}^{\text{enc}}$ to get the fusion feature $\hat{\mathbf{F}} \in \mathbb{R}^{\hat{D} \times \hat{H} \times \hat{W} \times \hat{d}_{\text{F}}}$ with \hat{d}_{F} feature dimensions,

$$\hat{\mathbf{F}} = f_{\text{fusion}}^{\text{enc}}([\mathbf{P}, \mathbf{I}]). \quad (3)$$

Loss Function. To guide $f_{\mathbf{P}}^{\text{enc}}$, $f_{\mathbf{I}}^{\text{enc}}$ and $f_{\text{fusion}}^{\text{enc}}$ to learn good representations in an unsupervised manner, CLAP first embed the fusion features $\hat{\mathbf{F}}$ with a shallow 3D convolution network $f^{3\text{D}}$ to get $\tilde{\mathbf{F}} = f^{3\text{D}}(\hat{\mathbf{F}})$ and we have $\tilde{\mathbf{F}} \in \mathbb{R}^{\hat{D} \times \hat{H} \times \hat{W} \times \hat{d}_{\text{F}}}$. Then a rendering loss $\mathcal{L}_{\text{rend}}$ is applied on $\tilde{\mathbf{F}}$ for masked-reconstruction on both point clouds \mathbf{P} and images \mathcal{I} . Furthermore, a prototype learning scheme $\mathcal{L}_{\text{proto}}$ is utilized in order to bridge the two modalities and incorporate interaction of image semantics and LiDAR geometry into pre-training. The overall loss function is as below:

$$\mathcal{L} = \omega_r \times \mathcal{L}_{\text{rend}}(\mathbf{P}, \tilde{\mathbf{F}}, \mathcal{I}) + \omega_{\text{proto}} \times \mathcal{L}_{\text{proto}}(\hat{\mathbf{P}}, \hat{\mathbf{I}}), \quad (4)$$

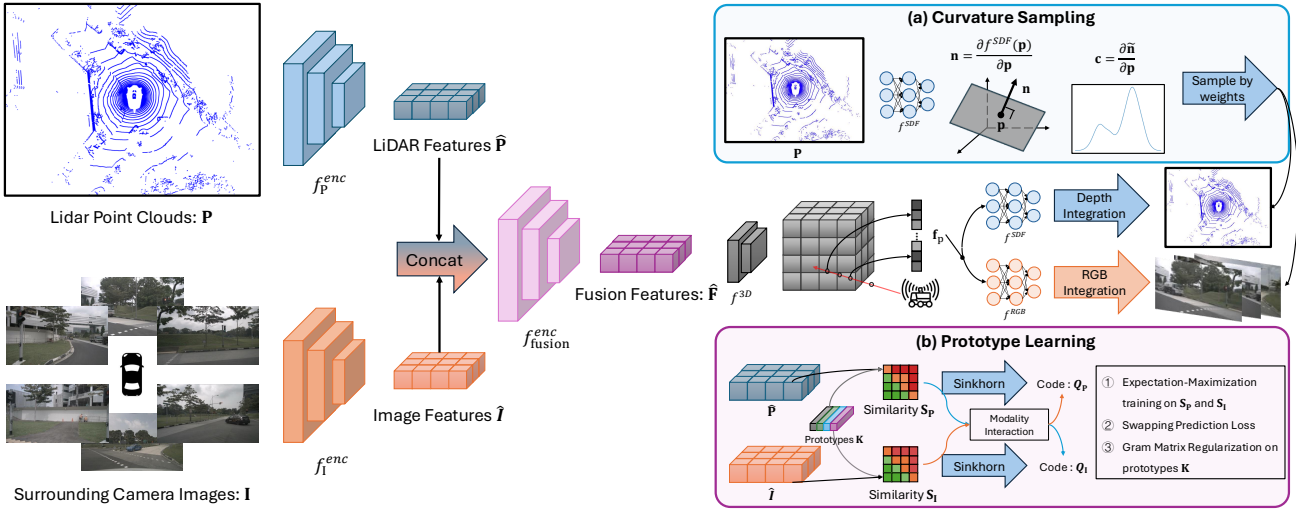


Figure 2. The pipeline of CLAP. In order to jointly pre-train the LiDAR, camera and fusion encoders, we first embed the paired LiDAR point clouds and camera images with f_P^{enc} , f_I^{enc} and f_{fusion}^{enc} . Then based on the fusion features, CLAP applies differentiable rendering to predict both depth and rgb with the SDF and RGB values of the sampled points along LiDAR/camera rays from f^{SDF} and f^{RGB} , with which we compute loss against the observed LiDAR point cloud and camera images. To make joint pre-training feasible, we propose Curvature Sampling to sample informative parts of the 3D scene, as described in (a). Furthermore, we propose to use learnable prototypes to represent parts of objects in a common feature space and utilize an Expectation-Maximization approach to maximize the similarity between prototypes and 3D embeddings of each modality. To delve deeper into the interplay of image semantics and LiDAR geometry, we use swapping prototype prediction loss. Finally, we propose a Gram Matrix Regularization loss to prevent collapse of prototype learning.

with ω_r and ω_{proto} as weighting parameters to balance the losses.

3.2. Neural Field and Differentiable Rendering

Inspired by the success of UniPAD [58], CLAP applies a differentiable rendering decoder with neural field to conduct the masked-and-reconstruction pre-training. Different from [58], an additional surface signed distance field loss is applied to better optimize the scene geometry. Here we first introduce Neural Field, which is the basis for camera images and point clouds rendering, and then discuss the differentiable rendering process on depth and RGB values.

Neural Field. Given a specific point $\mathbf{p} = [x, y, z] \in \mathbb{R}^3$ in the 3D space, the feature $\mathbf{f}_p \in \mathbb{R}^{d_F}$ at \mathbf{p} is queried from the fusion 3D embedding $\tilde{\mathbf{F}}$ by trilinear interpolation

$$\mathbf{f}_p = f^{\text{tri}}(\mathbf{p}, \hat{\mathbf{P}}_t), \quad (5)$$

where f^{tri} is an built-in module implemented in Pytorch [37]. Taking the concatenation of location \mathbf{p} and queried feature \mathbf{f}_p as inputs, we predict the signed distance value $s \in \mathbb{R}$ [5, 31] and color value $c \in \mathbb{R}^3$ [49] at \mathbf{p} with f^{SDF} and f^{RGB} .

$$s = f^{SDF}([\mathbf{p}, \mathbf{f}]), \quad c = f^{RGB}([\mathbf{p}, \mathbf{f}]), \quad (6)$$

where f^{RGB} and f^{SDF} are parameterized by Multi-layer Perceptron.

Differentiable Rendering. Similar to [33, 49], we first sample N_L or N_C rays at the LiDAR or camera sensor origin \mathbf{o} , each of which is described by its normalized direction \mathbf{d} and \mathbf{o} . Next, we sample N_{ray} points following [49] along each ray. Here each point along the ray can be interpreted by $\mathbf{p} = \mathbf{o} + r\mathbf{d}$, where r is the range from the sensor origin to the point \mathbf{p} . Thus the sampled point set can be annotated by $\{\mathbf{p}_n = \mathbf{o} + r_n \mathbf{d}\}_{n=1}^{N_{\text{ray}}}$ and we predict the estimated signed distance value s_n and color value c_n for them with f^{RGB} and f^{SDF} . Following [49], we estimate the occupancy value α_n for each sampled point,

$$\alpha_n = \max\left(\frac{\Phi_h(s_n) - \Phi_h(s_{n+1})}{\Phi_h(s_n)}, 0\right). \quad (7)$$

Here $\Phi_h(x) = (1+e^{-hx})^{-1}$ stands for the sigmoid function paired with a learnable scalar h . After that, we predict the accumulated transmittance t_n similar to [49]

$$t_n = \prod_{i=1}^{n-1} (1 - \alpha_i). \quad (8)$$

Based on t_n , we compute an unbiased and occlusion-aware weight $w_n = t_n \alpha_n$ [49] and integrate all samples along the ray to predict the range \tilde{r} or color \tilde{c} along this ray,

$$\tilde{r} = \sum_{n=1}^{N_{\text{ray}}} w_n * r_n, \quad \tilde{c} = \sum_{n=1}^{N_{\text{ray}}} w_n * c_n \quad (9)$$

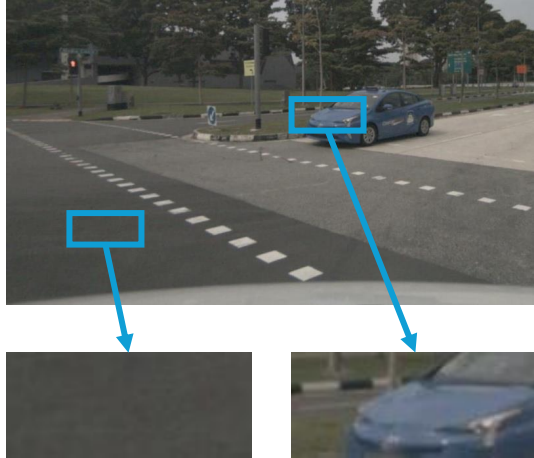


Figure 3. Inspiration of Curvature Sampling. It can be found that areas with low curvature tend to be less informative, like road plane, while those with high curvature provide more information (objects like cars).

For the observed LiDAR points, it is evident that signed distance value at those points are 0. The final loss function for differentiable rendering is a combination of L-1 loss on range and color predictions and the surface SDF loss.

$$\mathcal{L}_{\text{rend}} = \frac{1}{N_L} \sum_{i=1}^{N_L} (|r_i - \tilde{r}_i| + \omega_{\text{sur}} |s_i|) + \frac{\omega_C}{3 \cdot N_C} \sum_{i=1}^{N_C} \sum_{j=1}^3 |c_i^j - \tilde{c}_i^j| \quad (10)$$

where ω_{sur} and ω_C are weighting parameters for the losses. r_i is the observed range along the i^{th} sampled ray and s_i is the predicted signed distance value at the observed points. c_i^j is the value of j^{th} channel in the image pixel, where $j = \{1, 2, 3\}$ corresponds to RGB channels.

3.3. Curvature Sampling

In order to make joint unsupervised representation learning feasible, we have to make $N_L \ll N_P$ and $N_C \ll H \cdot W \cdot N_{\text{cam}}$. Intuitively, uniform sampling with depth can be used, same as “Memory-friendly Ray Sampling” in [58]. But due to the relatively small sample number compared to the raw inputs ($\sim \frac{1}{100}$), this sampling method brings little improvement against separate pre-training, which is contradictory to our motivation. Hence, we need to sample more informative part of the scene for $\mathcal{L}_{\text{rend}}$. As shown in Figure 3, we are inspired by the observation that surface with higher curvature (surface of a vehicle) generally contains more information as compared to that with lower curvature (road plane). Therefore, we propose the Curvature Sampling for effective sampling. For each point \mathbf{p} in the LiDAR point cloud \mathbf{P} , we first estimate the surface normal by deriving the signed distance function with respect to \mathbf{p}

$$\mathbf{n} = \frac{\delta f^{\text{SDF}}([\mathbf{p}, \mathbf{f}])}{\delta \mathbf{p}}, \quad (11)$$

where $\mathbf{n} \in \mathbb{R}^3$ is the predicted normal. Then we normalized \mathbf{n} to get the direction of the normal $\tilde{\mathbf{n}} = \frac{\mathbf{n}}{\|\mathbf{n}\|_2}$. Here $\|\cdot\|_2$ is the L-2 norm. Next we apply the differential operator on $\tilde{\mathbf{n}}$ with respect to \mathbf{p} and get $\mathbf{c} \in \mathbb{R}^3$.

$$\mathbf{c} = \frac{\delta \tilde{\mathbf{n}}}{\delta \mathbf{p}}. \quad (12)$$

Then we estimate the geodesic curvature [48] of each point \mathbf{p}_n in LiDAR point cloud by computing the norm of \mathbf{c}_n and use it as the sampling weights ω_n , that is $\omega_n = \|\mathbf{c}_n\|_2$. With ω_n , we sample N_L points with a Multinomial Sampler implemented in PyTorch [37] for differentiable rendering. For pixels on image plane, we project the LiDAR point cloud back to image planes with \mathcal{T} , assign ω_n of each point to the projected pixel and apply a gaussian blur kernel of size K_{gaus} to densify the weights, with which we sample N_C pixels for $\mathcal{L}_{\text{rend}}$. As the estimation of curvature here is noisy especially in the first few epochs, we set up a warm-up stage with N_{warmup} epochs with uniform sampling and after N_{warmup} epochs, Curvature Sampling is utilized.

3.4. Prototype Learning

Curvature Sampling allows for joint pre-training, prompting us to explore how camera and LiDAR data can be used to understand “objectness” or “object parts” in an unsupervised way. We use learnable prototypes to represent segments of 3D scenes and establish a shared feature space that connects the two modalities. Firstly, we randomly initialize N_K learnable prototypes $\mathbf{K} \in \mathbb{R}^{N_K \times d_K}$, each of which is a d_K vectors. Then an Expectation-Maximization training approach is proposed to maximize the similarity between these prototypes and 3D embeddings from the two modalities. To delve deeper into the interplay between image semantics and LiDAR geometry, we use the swapping prototype prediction loss. Finally, to avoid the prototype collapsing into one same vector, we introduce a Gram Matrix Regularization Loss.

Expectation-Maximization. In order to guide the learnable prototypes to represent parts of the environment, we propose an Expectation-Maximization [35] training scheme to optimize the prototypes. We first project the LiDAR embeddings $\hat{\mathbf{P}}$ and camera embeddings $\hat{\mathbf{I}}$ separately with two projection heads $f_{\mathbf{P}}^{\text{proj}}$ and $f_{\mathbf{I}}^{\text{proj}}$ to the same dimension as \mathbf{K}

$$\hat{\mathbf{P}} = f_{\mathbf{P}}^{\text{proj}}(\hat{\mathbf{P}}) \quad , \quad \hat{\mathbf{I}} = f_{\mathbf{I}}^{\text{proj}}(\hat{\mathbf{I}}), \quad (13)$$

where $f_{\mathbf{P}}^{\text{proj}}$ and $f_{\mathbf{I}}^{\text{proj}}$ are parameterized by Multi-Layer Perceptron and $\hat{\mathbf{P}} \in \mathbb{R}^{\hat{D} \times \hat{H} \times \hat{W} \times d_K}$, $\hat{\mathbf{I}} \in \mathbb{R}^{\hat{D} \times \hat{H} \times \hat{W} \times d_K}$. We denote $N_{3D} = \hat{D} \times \hat{H} \times \hat{W}$ and then normalize and reshape the projected embeddings into $\hat{\mathbf{P}} \in \mathbb{R}^{N_{3D} \times d_K}$ and $\hat{\mathbf{I}} \in \mathbb{R}^{N_{3D} \times d_K}$. After that, similarity scores $\mathbf{S}_{\mathbf{P}/\mathbf{I}} \in \mathbb{R}^{N_{3D} \times N_K}$ between 3D embeddings and prototypes are computed separately for Li-

DAR and camera branches

$$\mathbf{S}_P = \dot{\mathbf{P}} \cdot \mathbf{K}^\top, \quad \mathbf{S}_I = \dot{\mathbf{I}} \cdot \mathbf{K}^\top. \quad (14)$$

In the Expectation step, we compute the probability $\hat{\mathbf{S}}_{P/I}$ that each prototype is assigned to each embeddings by applying a softmax operation on $\mathbf{S}_{P/I}$. Then for Maximization step, we expect to maximize the probability of the assignment between one prototype to one specific part of the scene and this is the same as minimizing the entropy of the similarity matrix. Hence, the EM loss is computed as,

$$\mathcal{L}_{EM} = -\frac{1}{N_{3D}N_K} \sum_{n=1}^{N_{3D}} \sum_{m=1}^{N_K} \{\hat{\mathbf{S}}_P^{n,m} \log \hat{\mathbf{S}}_P^{n,m} + \hat{\mathbf{S}}_I^{n,m} \log \hat{\mathbf{S}}_I^{n,m}\} \quad (15)$$

Swapping Prototype Prediction. To further explore interaction between modalities, we detach $\mathbf{S}_{P/I}$ and apply sinkhorn algorithm [9] to make them approximate to double stochastic matrix in N_{sink} iterations. We denote the updated matrix as codes $\mathbf{Q}_{P/I} \in \mathbb{R}^{N_{3D} \times N_K}$. The swapping prototype prediction loss is formulated with a temperature parameter τ , inspired by [4],

$$\begin{aligned} \mathcal{L}_{SwAV} = & -\frac{1}{N_{3D}N_K} \sum_{n=1}^{N_{3D}} \sum_{m=1}^{N_K} \{\mathbf{Q}_I^{n,m} \log \frac{\exp(\mathbf{S}_P^{n,m})/\tau}{\sum_{k=1}^{N_K} \exp(\mathbf{S}_P^{n,k})/\tau} \\ & + \mathbf{Q}_P^{n,m} \log \frac{\exp(\mathbf{S}_I^{n,m})/\tau}{\sum_{k=1}^{N_K} \exp(\mathbf{S}_I^{n,k})/\tau}\}. \end{aligned} \quad (16)$$

Gram Matrix Minimization. When training the randomly initialized prototypes, the network might learn a short cut with all prototypes being the same [4], which is called collapse. To avoid this, we estimate similarity between prototypes by the gram matrix $\mathbf{G} = \mathbf{K}\mathbf{K}^\top$ of prototypes \mathbf{K} , the dimension of which is $\mathbf{G} \in \mathbb{R}^{N_K \times N_K}$. Finally we minimize the average of the non-diagonal elements of \mathbf{G} in order to avoid collapse

$$\mathcal{L}_{GMM} = \frac{1}{N_K(N_K - 1)} \sum_n^{N_K} \sum_{m=1, m \neq n}^{N_K} \mathbf{G}^{n,m}. \quad (17)$$

Overall Prototype Learning Loss. We apply weighting parameters ω_{SwAV} , ω_{EM} and ω_{GMM} to balance the three losses proposed above, which leads to the overall loss function for prototype learning,

$$\mathcal{L}_{proto} = \omega_{SwAV} \mathcal{L}_{SwAV} + \omega_{EM} \mathcal{L}_{EM} + \omega_{GMM} \mathcal{L}_{GMM}. \quad (18)$$

4. Experiments

Unsupervised 3D representation learning for fusion perception aims to pre-train both LiDAR and camera encoders and

initialize downstream models with the pre-trained weights to gain performance improvement in downstream tasks. In this section, we design extensive experiments on the popular autonomous driving dataset NuScenes [3] and Waymo [45] to demonstrate the effectiveness of CLAP. To begin with, we describe experiment setups in Section 4.1. Next, we show and analyze main results in Section 4.2. Finally, we provide ablation study and visualizations separately in Section 4.3 and 4.4.

4.1. Settings

Datasets. We use the popular autonomous driving dataset NuScenes [3] and Waymo [45] to evaluate the performance of CLAP. NuScenes [3] uses one roof LiDAR and six surrounding cameras to collect data. The LiDAR is a 32-beam Velodyne and collecting frequency is 20Hz. The frequency of camera capturing is 12Hz. [3] conducts the synchronization and provides paired data of LiDAR point cloud and camera images. The whole NuScenes dataset contains 1000 scenes collected in Boston and Singapore. Each scene lasts for around 20 seconds and there are a total of 5.5 hours data. Following convention practice from [3, 46], we divide the whole dataset into training set with 850 scenes and validation set with 150 scenes. Waymo [45] uses one top 64-beam LiDAR, 4 corner LiDARs and 5 surrounding cameras to collect point clouds and camera images. Following the same practice in [45, 46], the collected 1000 scenes are split into training set (798 scenes) and validation set (202 scenes). All pre-trainings are conducted on the training set without labels and we conduct downstream 3D object detection training in few-shot setting via uniform sampling of the training data (NuScenes [3] 5% and Waymo [45] 1%).

Downstream 3D Object Detectors. For NuScenes [3], we select the SOTA 3D object detector called BEVFusion [30] and for Waymo [45], we use CenterPoint [59]. Both BEVFusion and CenterPoint are implemented in the popular code repository for autonomous driving perception called OpenPCDet [46]. For evaluation metrics, we use average precisions of various categories (APs), mean average precision (mAP) and NuScenes Detection Score (NDS) [3] for NuScenes [3] and mAP (mean accurate precisions) and mAPH (mean accurate precisions with headings) at different difficulty levels (Level-1 and 2) for Waymo [45]. We follow a similar setting in [14, 53] to gradually increase training iterations of the from-scratch model until convergence is observed. Here convergence means further increasing training iterations will not improve the performance. Then the number of training iterations is fixed for fine-tuning pre-trained models. This setting *avoids the case that pre-training only accelerates convergence and makes sure that pre-training indeed improve the performance of downstream models*, that is improving the sample efficiency of the downstream task.

Init.	mAP	NDS	Car	Truck	C.V.	Bus	Trailer	Barrier	Mot.	Bic.	Ped.	T.C.
Rand.	48.69	55.28	78.52	46.64	16.18	50.44	22.11	57.00	46.87	30.56	76.16	62.40
ALSO	45.34 <small>-3.35</small>	49.19 <small>-6.09</small>	77.61	41.98	14.61	36.09	12.55	58.10	42.89	30.56	74.09	64.98
OCC-MAE	47.39 <small>-1.30</small>	54.97 <small>-0.31</small>	77.43	46.25	15.26	50.06	19.35	55.35	43.24	30.92	74.69	61.34
SLidR	47.23 <small>-1.46</small>	52.77 <small>-2.51</small>	77.12	45.04	16.19	50.50	22.17	57.74	41.47	30.22	71.11	60.71
PPKT	49.58 <small>+0.89</small>	55.85 <small>+0.57</small>	79.24	47.26	17.26	51.37	21.14	59.55	44.82	31.43	78.03	65.73
UniPAD	49.81 <small>+1.12</small>	55.29 <small>+0.01</small>	80.81	42.81	17.08	48.98	25.85	61.72	50.19	27.53	78.53	64.57
CLAP	51.17 <small>+2.48</small>	57.04 <small>+1.76</small>	79.56	48.43	18.84	56.34	23.98	60.60	48.87	34.11	78.08	62.87

Table 1. Results for fine-tuning on 5% of training set in NuScenes [3]. “Init.” means the way to initialize models. To avoid the case the performance difference is brought by accelerating convergence, we first increase the training iteration of training-from-scratch model (BEVFusion [30]) until we observe convergence, which leads to the “Rand.” row. Then we pre-train the backbones with ALSO [2], OCC-MAE [34], SLidR [38], PPKT [28], UniPAD [58] and CLAP. We initialize BEVFusion with the pre-trained weights and fine-tune the model with the same number iterations as “Rand.”. We provide mAP and NDS as an evaluation of the overall performance of different models and highlight the best mAP and NDS with bold font. We also indicate the performance improvement by green color. “C.V.”, “Mot.”, “Bic.”, “Ped.” and “T.C.” are abbreviations for Construction Vehicle, Motorcycle, Bicycle, Pedestrian and Traffic Cone. All the results here are in %.

Baseline Pre-training Method for Fusion Perception. We incorporate three kinds of pre-training baseline methods: 1) an occupancy estimation method called ALSO [2], 2) occupancy masked autoencoder called Occupancy-MAE [34], 3) multi-modality methods including SLidR [38], PPKT [28] and UniPAD [58]. We use the official implementations to pre-train the backbones with same setting as CLAP.

Implementation Details of CLAP. The feature channels for embeddings $\hat{\mathbf{P}}$, $\hat{\mathbf{I}}$, $\hat{\mathbf{F}}$ and prototypes \mathbf{K} are respectively set to $\hat{d}_{\mathbf{P}} = 256$, $\hat{d}_{\mathbf{I}} = 80$, $\hat{d}_{\mathbf{F}} = 512$ and $\hat{d}_{\mathbf{K}} = 128$. Sampling number for point cloud and pixel are $N_{\mathbf{L}} = 8192$ and $N_{\mathbf{C}} = 1024 \times N_{\text{cam}}$. The number of sample points along each ray is $N_{\text{ray}} = 96$. Warm-up epochs for Curvature Sampling is $N_{\text{warmup}} = 4$. We set the number of learnable prototypes and sinkhorn update iterations to $N_{\mathbf{K}} = 512$ and $N_{\text{sink}} = 3$. The temperature for swapping prediction loss is $\tau = 1.0$. The loss weighting parameters are implemented as $\omega_r = 2.0$, $\omega_{\text{proto}} = 1.0$, $\omega_{\text{sur}} = 0.05$, $\omega_{\mathbf{C}} = 0.05$, $\omega_{\text{SwAV}} = 1.0$, $\omega_{\text{EM}} = 0.1$ and $\omega_{\text{GMM}} = 0.1$. We use `torch.auto_grad()` [37] to implement the derivatives in the curvature estimation. For more details about pre-training and fine-tuning, please refer to Appendix 1.

4.2. Main Results

NuScenes Results. As shown in Table 1, CLAP achieves 2.48% mAP improvement over randomly initialization at convergence, which is 100% more improvement for mAP than SOTA unsupervised 3D representation method UniPAD [58] and the best among all initialization methods. For NDS metric, UniPAD [58] only achieves comparable performance and PPKT [28] makes a gain of 0.57% while CLAP surpasses the train-from-scratch model by 1.76%. When it turns to different categories, CLAP generally benefit the performance of all the categories and for Construction Vehicle, Bus, Barrier, Motorcycle and Bicycle, the improvement over random initialization are more than 2% AP.

Waymo Results. In Table 2, we provide the average performance difference of mAP and mAPH over different dif-

Init.	Level-1		Level-2		$\bar{\Delta}$
	mAP	mAPH	mAP	mAPH	
Rand.	61.60	58.58	55.62	52.87	0
ALSO	62.09	59.03	56.12	53.32	<small>+0.47</small>
OCC-MAE	62.33	59.32	56.36	53.63	<small>+0.74</small>
SLidR	62.10	59.09	56.10	53.36	<small>+0.49</small>
PPKT	62.32	59.22	56.37	53.55	<small>+0.69</small>
UniPAD	61.57	58.64	55.64	52.93	<small>+0.02</small>
CLAP	62.87	59.88	56.88	54.16	<small>+1.28</small>

Table 2. Results for fine-tuning on 1% of training set in Waymo [45]. We first increase training iterations of from-scratch model and observe convergence (Rand.). Then we fix the training schedule to fine-tune the pre-training models. We provide an average difference $\bar{\Delta}$ to show the performance gain. All results are in %.

ficulty levels. It can be found that CLAP achieves the best performance at convergence. Meanwhile, the performance gain brought by CLAP is approximately two times as the best (OCC-MAE [34]) of previous pre-training methods. This demonstrates the effectiveness and generalization ability of CLAP.

Potential Scaling Property. As we are not able to scale up the pre-training dataset at current stage, we explore potential scaling property by gradually decreasing the sample numbers (2.5%, 1% and 0.5%) for fine-tuning on NuScenes, which increases the ratio between pre-training data and fine-tuning data. The results are shown in Table 3. It can be found that as the ratio between pre-training data and fine-tuning data gets larger, the performance improvement by CLAP increases and CLAP provides a gain up to 7.22% mAP and 4.71% NDS with 0.5% fine-tuning data. These results show that CLAP is promising in scaling property and in the future, if we can scale up the pre-training dataset, CLAP might further improve current SOTA performance.

4.3. Visualizations

We use the pre-trained model to estimate the curvature of LiDAR point clouds and use heatmap color to indicate the

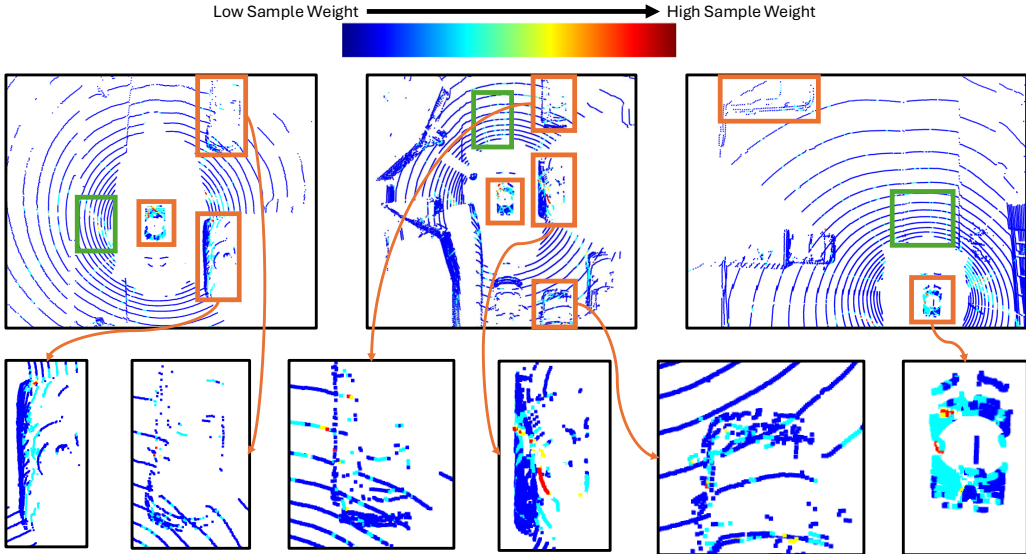


Figure 4. Visualization of curvature estimation. The color of the points change from blue to red, indicating lower sample weight / curvature to higher ones. We highlight those correct regions with orange boxes and those noisy estimation with green ones. Some of the correct estimated regions are further zoom-in for better understanding. Best view in color.

Init.	Fine-tune Data	mAP	NDS
Random	5%	48.69	55.28
CLAP		51.17 +2.48	57.04 +1.76
Random	2.5%	39.12	40.01
CLAP		42.86 +3.74	42.18 +2.17
Random	1%	26.22	29.82
CLAP		30.53 +4.31	31.87 +2.05
Random	0.5%	16.49	22.61
CLAP		23.71 +7.22	27.32 +4.71

Table 3. Results on potential scaling property of CLAP . ‘‘Fine-tune Data’’ stands for the sample number of training set in NuScenes [3]. Results for random initialization are at convergence and fine-tuning with CLAP uses the same numbers of iterations. Results are mAP and NDS in %.

weight computed in Section 3.3. The visualization results are shown in Figure 4. We use orange boxes to highlight those regions with relatively correct estimation and green ones for those with noisy estimation. Furthermore, we zoom in some orange boxes. It can be found that though some noise exists (because pre-training is conducted in unsupervised manner), CLAP is able to predict high weights for those highly informative region for sampling and meanwhile assign lower weights to most of the background, which makes joint pre-training feasible.

4.4. Ablation Study

We conduct ablation study to evaluate the effectiveness of different components. Results are in Table 4. The first line is separate pre-training with UniPAD [58]. The second one is jointly pre-training using UniPAD [58] and uniform sam-

Joint Pre-train	Cur. Sam.	Proto. Learning	mAP
✗	✗	✗	49.81
✓	✗	✗	49.55
✓	✓	✗	50.81
✓	✓	✓	51.17

Table 4. Results for ablation study. We use BEVFusion [30] as the downstream model. Results are mAPs in %.

pling guided by depth (“Memory-friendly Ray Sampling” in [58]) to address the GPU memory limitation. It can be found that using simple sampling method does not bring improvement over separate pre-training. Then we add Curvature Sampling in third line and found that Curvature Sampling enables more effective sampling and improves the performance over uniform sampling guided by depth and separate pre-training. Finally, the Prototype Learning scheme (fourth line) learns a common feature space for segments of 3D scenes and introduces interaction of LiDAR and camera encoders, which achieves the best performance.

5. Conclusion

In this paper, we propose CLAP for unsupervised fusion joint pre-training via differentiable rendering. CLAP uses Curvature Sampling to sample more informative parts and learnable prototypes to represent parts of 3D scenes, optimized with an Expectation-Maximization approach. To further make use of the interplay between LiDAR geometry and image semantics, a swapping prediction loss is used. Finally, a Gram Matrix Regularization loss is proposed to avoid collapse. Experiment results demonstrate that CLAP is superior in unsupervised 3D representation learning and has the potential to scale up.

References

- [1] Xuyang Bai, Zeyu Hu, Xinge Zhu, Qingqiu Huang, Yilun Chen, Hongbo Fu, and Chiew-Lan Tai. Transfusion: Robust lidar-camera fusion for 3d object detection with transformers. In *Proceedings of the IEEE/CVF conference on computer vision and pattern recognition*, pages 1090–1099, 2022. [1](#) [2](#)
- [2] Alexandre Boulch et al. ALSO: Automotive lidar self-supervision by occupancy estimation. In *CVPR*, 2023. [7](#)
- [3] Holger Caesar, Varun Bankiti, Alex H Lang, Sourabh Vora, Venice Erin Liang, Qiang Xu, Anush Krishnan, Yu Pan, Giacomo Baldan, and Oscar Beijbom. nuscenes: A multi-modal dataset for autonomous driving. In *Proceedings of the IEEE/CVF Conference on Computer Vision and Pattern Recognition*, pages 11621–11631, 2020. [2](#) [3](#) [6](#) [7](#) [8](#)
- [4] Mathilde Caron, Ishan Misra, Julien Mairal, Priya Goyal, Piotr Bojanowski, and Armand Joulin. Unsupervised learning of visual features by contrasting cluster assignments. In *Advances in Neural Information Processing Systems*, pages 9912–9924. Curran Associates, Inc., 2020. [2](#) [3](#) [6](#)
- [5] Tony Chan and Wei Zhu. Level set based shape prior segmentation. In *2005 IEEE Computer Society Conference on Computer Vision and Pattern Recognition (CVPR'05)*, pages 1164–1170. IEEE, 2005. [4](#)
- [6] Runjian Chen, Yao Mu, Runsen Xu, Wenqi Shao, Chenhan Jiang, Hang Xu, Zhenguo Li, and Ping Luo. Co³: Cooperative unsupervised 3d representation learning for autonomous driving. *arXiv preprint arXiv:2206.04028*, 2022. [2](#)
- [7] Xiaozhi Chen, Kaustav Kundu, Ziyu Zhang, Huimin Ma, Sanja Fidler, and Raquel Urtasun. Monocular 3d object detection for autonomous driving. In *Proceedings of the IEEE conference on computer vision and pattern recognition*, pages 2147–2156, 2016. [1](#) [2](#)
- [8] Xiaozhi Chen, Huimin Ma, Ji Wan, Bo Li, and Tian Xia. Multi-view 3d object detection network for autonomous driving. In *Proceedings of the IEEE conference on Computer Vision and Pattern Recognition*, pages 1907–1915, 2017. [1](#) [2](#)
- [9] Marco Cuturi. Sinkhorn distances: Lightspeed computation of optimal transport. *Advances in neural information processing systems*, 26, 2013. [6](#)
- [10] Jiajun Deng, Shaoshuai Shi, Peiwei Li, Wengang Zhou, Yanyong Zhang, and Houqiang Li. Voxel r-cnn: Towards high performance voxel-based 3d object detection. In *Proceedings of the AAAI conference on artificial intelligence*, pages 1201–1209, 2021. [2](#)
- [11] Mingyu Ding, Yuqi Huo, Hongwei Yi, Zhe Wang, Jianping Shi, Zhiwu Lu, and Ping Luo. Learning depth-guided convolutions for monocular 3d object detection. In *Proceedings of the IEEE/CVF Conference on computer vision and pattern recognition workshops*, pages 1000–1001, 2020. [1](#) [2](#)
- [12] Lue Fan, Ziqi Pang, Tianyuan Zhang, Yu-Xiong Wang, Hang Zhao, Feng Wang, Naiyan Wang, and Zhaoxiang Zhang. Embracing single stride 3d object detector with sparse transformer. *arXiv preprint arXiv:2112.06375*, 2021. [1](#) [2](#)
- [13] Jean-Bastien Grill, Florian Strub, Florent Altché, Corentin Tallec, Pierre Richemond, Elena Buchatskaya, Carl Doersch, Bernardo Avila Pires, Zhaohan Guo, Mohammad Gheshlaghi Azar, Bilal Piot, koray kavukcuoglu, Remi Munos, and Michal Valko. Bootstrap your own latent - a new approach to self-supervised learning. In *Advances in Neural Information Processing Systems*, pages 21271–21284. Curran Associates, Inc., 2020. [2](#)
- [14] Kaiming He, Ross Girshick, and Piotr Dollár. Rethinking imagenet pre-training. In *Proceedings of the IEEE/CVF international conference on computer vision*, pages 4918–4927, 2019. [6](#)
- [15] Kaiming He, Haoqi Fan, Yuxin Wu, Saining Xie, and Ross Girshick. Momentum contrast for unsupervised visual representation learning. In *Proceedings of the IEEE/CVF Conference on Computer Vision and Pattern Recognition*, pages 9729–9738, 2020. [2](#)
- [16] Kaiming He, Xinlei Chen, Saining Xie, Yanghao Li, Piotr Dollár, and Ross Girshick. Masked autoencoders are scalable vision learners. In *Proceedings of the IEEE/CVF conference on computer vision and pattern recognition*, pages 16000–16009, 2022. [2](#)
- [17] Ji Hou, Benjamin Graham, Matthias Nießner, and Saining Xie. Exploring data-efficient 3d scene understanding with contrastive scene contexts. In *Proceedings of the IEEE/CVF conference on computer vision and pattern recognition*, pages 15587–15597, 2021. [2](#)
- [18] Di Huang, Sida Peng, Tong He, Honghui Yang, Xiaowei Zhou, and Wanli Ouyang. Ponder: Point cloud pre-training via neural rendering. In *Proceedings of the IEEE/CVF International Conference on Computer Vision*, pages 16089–16098, 2023. [2](#) [3](#)
- [19] Siyuan Huang, Yichen Xie, Song-Chun Zhu, and Yixin Zhu. Spatio-temporal self-supervised representation learning for 3d point clouds. In *Proceedings of the IEEE/CVF International Conference on Computer Vision*, pages 6535–6545, 2021. [2](#)
- [20] Jason Ku, Alex D Pon, and Steven L Waslander. Monocular 3d object detection leveraging accurate proposals and shape reconstruction. In *Proceedings of the IEEE/CVF conference on computer vision and pattern recognition*, pages 11867–11876, 2019. [1](#) [2](#)
- [21] Yanwei Li, Xiaojuan Qi, Yukang Chen, Liwei Wang, Zeming Li, Jian Sun, and Jiaya Jia. Voxel field fusion for 3d object detection. In *Proceedings of the IEEE/CVF Conference on Computer Vision and Pattern Recognition*, pages 1120–1129, 2022. [1](#) [2](#)
- [22] Yingwei Li, Adams Wei Yu, Tianjian Meng, Ben Caine, Jiquan Ngiam, Daiyi Peng, Junyang Shen, Yifeng Lu, Denny Zhou, Quoc V Le, et al. Deepfusion: Lidar-camera deep fusion for multi-modal 3d object detection. In *Proceedings of the IEEE/CVF conference on computer vision and pattern recognition*, pages 17182–17191, 2022. [1](#) [2](#)
- [23] Zhenyu Li, Zehui Chen, Ang Li, Liangji Fang, Qinzhong Jiang, Xianming Liu, Junjun Jiang, Bolei Zhou, and Hang Zhao. Simipu: Simple 2d image and 3d point cloud unsupervised pre-training for spatial-aware visual representations. In *Proceedings of the AAAI Conference on Artificial Intelligence*, pages 1500–1508, 2022. [2](#)

[24] Hanxue Liang, Chenhan Jiang, Dapeng Feng, Xin Chen, Hang Xu, Xiaodan Liang, Wei Zhang, Zhenguo Li, and Luc Van Gool. Exploring geometry-aware contrast and clustering harmonization for self-supervised 3d object detection. In *Proceedings of the IEEE/CVF International Conference on Computer Vision*, pages 3293–3302, 2021. 2

[25] Ming Liang, Bin Yang, Yun Chen, Rui Hu, and Raquel Urtasun. Multi-task multi-sensor fusion for 3d object detection. In *Proceedings of the IEEE/CVF conference on computer vision and pattern recognition*, pages 7345–7353, 2019. 1, 2

[26] Tingting Liang, Hongwei Xie, Kaicheng Yu, Zhongyu Xia, Zhiwei Lin, Yongtao Wang, Tao Tang, Bing Wang, and Zhi Tang. Bevfusion: A simple and robust lidar-camera fusion framework. *Advances in Neural Information Processing Systems*, 35:10421–10434, 2022. 1, 2

[27] Yunze Liu, Li Yi, Shanghang Zhang, Qingnan Fan, Thomas Funkhouser, and Hao Dong. P4contrast: Contrastive learning with pairs of point-pixel pairs for rgb-d scene understanding. *arXiv preprint arXiv:2012.13089*, 2020. 2

[28] Yueh-Cheng Liu et al. Learning from 2d: Contrastive pixel-to-point knowledge transfer for 3d pretraining. *arXiv preprint arXiv:2104.04687*, 2021. 2, 7

[29] Ze Liu, Yutong Lin, Yue Cao, Han Hu, Yixuan Wei, Zheng Zhang, Stephen Lin, and Baining Guo. Swin transformer: Hierarchical vision transformer using shifted windows. In *Proceedings of the IEEE/CVF international conference on computer vision*, pages 10012–10022, 2021. 3

[30] Zhijian Liu, Haotian Tang, Alexander Amini, Xinyu Yang, Huizi Mao, Daniela L Rus, and Song Han. Bevfusion: Multi-task multi-sensor fusion with unified bird’s-eye view representation. In *2023 IEEE international conference on robotics and automation (ICRA)*, pages 2774–2781. IEEE, 2023. 1, 2, 3, 6, 7, 8

[31] Ravi Malladi, James A Sethian, and Baba C Vemuri. Shape modeling with front propagation: A level set approach. *IEEE transactions on pattern analysis and machine intelligence*, 17(2):158–175, 1995. 4

[32] Gregory P Meyer, Jake Charland, Darshan Hegde, Ankit Laddha, and Carlos Valdes-Gonzalez. Sensor fusion for joint 3d object detection and semantic segmentation. In *Proceedings of the IEEE/CVF conference on computer vision and pattern recognition workshops*, pages 0–0, 2019. 1, 2

[33] Ben Mildenhall, Pratul P Srinivasan, Matthew Tancik, Jonathan T Barron, Ravi Ramamoorthi, and Ren Ng. Nerf: Representing scenes as neural radiance fields for view synthesis. *Communications of the ACM*, 65(1):99–106, 2021. 3, 4

[34] Chen Min et al. Occupancy-mae: Self-supervised pre-training large-scale lidar point clouds with masked occupancy autoencoders. *IEEE TIV*, 2023. 7

[35] Todd K Moon. The expectation-maximization algorithm. *IEEE Signal processing magazine*, 13(6):47–60, 1996. 5

[36] Bo Pang, Hongchi Xia, and Cewu Lu. Unsupervised 3d point cloud representation learning by triangle constrained contrast for autonomous driving. In *Proceedings of the IEEE/CVF Conference on Computer Vision and Pattern Recognition*, pages 5229–5239, 2023. 2

[37] Adam Paszke, Sam Gross, Francisco Massa, Adam Lerer, James Bradbury, Gregory Chanan, Trevor Killeen, Zeming Lin, Natalia Gimelshein, Luca Antiga, et al. Pytorch: An imperative style, high-performance deep learning library. *Advances in neural information processing systems*, 32, 2019. 4, 5, 7

[38] Corentin Sautier et al. Image-to-lidar self-supervised distillation for autonomous driving data. In *CVPR*, 2022. 2, 7

[39] Shaoshuai Shi, Xiaogang Wang, and Hongsheng Li. Pointrcnn: 3d object proposal generation and detection from point cloud. In *The IEEE Conference on Computer Vision and Pattern Recognition (CVPR)*, 2019. 1, 2

[40] Shaoshuai Shi, Chaoxu Guo, Li Jiang, Zhe Wang, Jianping Shi, Xiaogang Wang, and Hongsheng Li. Pv-rcnn: Point-voxel feature set abstraction for 3d object detection. In *Proceedings of the IEEE/CVF conference on computer vision and pattern recognition*, pages 10529–10538, 2020. 2

[41] Shaoshuai Shi, Zhe Wang, Jianping Shi, Xiaogang Wang, and Hongsheng Li. From points to parts: 3d object detection from point cloud with part-aware and part-aggregation network. *IEEE transactions on pattern analysis and machine intelligence*, 43(8):2647–2664, 2020. 2

[42] Shaoshuai Shi, Li Jiang, Jiajun Deng, Zhe Wang, Chaoxu Guo, Jianping Shi, Xiaogang Wang, and Hongsheng Li. Pv-rcnn++: Point-voxel feature set abstraction with local vector representation for 3d object detection. *arXiv preprint arXiv:2102.00463*, 2021. 1, 2

[43] Andrea Simonelli, Samuel Rota Bulo, Lorenzo Porzi, Manuel López-Antequera, and Peter Kotschieder. Disentangling monocular 3d object detection. In *Proceedings of the IEEE/CVF International Conference on Computer Vision*, pages 1991–1999, 2019. 1, 2

[44] Jiachen Sun, Haizhong Zheng, Qingzhao Zhang, Atul Prakash, Z Morley Mao, and Chaowei Xiao. Calico: Self-supervised camera-lidar contrastive pre-training for bev perception. *arXiv preprint arXiv:2306.00349*, 2023. 3

[45] Pei Sun, Henrik Kretzschmar, Xerxes Dotiwalla, Aurelien Chouard, Vijaysai Patnaik, Paul Tsui, James Guo, Yin Zhou, Yuning Chai, Benjamin Caine, et al. Scalability in perception for autonomous driving: Waymo open dataset. In *Proceedings of the IEEE/CVF Conference on Computer Vision and Pattern Recognition*, pages 2446–2454, 2020. 2, 6, 7

[46] OpenPCDet Development Team. Openpcdet: An open-source toolbox for 3d object detection from point clouds. <https://github.com/open-mmlab/OpenPCDet>, 2020. 6

[47] Yonglong Tian, Dilip Krishnan, and Phillip Isola. Contrastive multiview coding. *arXiv preprint arXiv:1906.05849*, 2019. 2

[48] Victor A Toponogov. *Differential geometry of curves and surfaces*. Springer, 2006. 5

[49] Peng Wang, Lingjie Liu, Yuan Liu, Christian Theobalt, Taku Komura, and Wenping Wang. Neus: Learning neural implicit surfaces by volume rendering for multi-view reconstruction. *arXiv preprint arXiv:2106.10689*, 2021. 3, 4

[50] Tai Wang, Xinge Zhu, Jiangmiao Pang, and Dahua Lin. Fcos3d: Fully convolutional one-stage monocular 3d object

detection. In *Proceedings of the IEEE/CVF International Conference on Computer Vision*, pages 913–922, 2021. [1](#), [2](#)

[51] Xinlong Wang, Rufeng Zhang, Chunhua Shen, Tao Kong, and Lei Li. Dense contrastive learning for self-supervised visual pre-training. In *Proc. IEEE Conf. Computer Vision and Pattern Recognition (CVPR)*, 2021. [2](#)

[52] Saining Xie, Jiatao Gu, Demi Guo, Charles R Qi, Leonidas Guibas, and Or Litany. Pointcontrast: Unsupervised pre-training for 3d point cloud understanding. In *Computer Vision–ECCV 2020: 16th European Conference, Glasgow, UK, August 23–28, 2020, Proceedings, Part III 16*, pages 574–591. Springer, 2020. [2](#)

[53] Runsen Xu, Tai Wang, Wenwei Zhang, Runjian Chen, Jinkun Cao, Jiangmiao Pang, and Dahua Lin. Mv-jar: Masked voxel jigsaw and reconstruction for lidar-based self-supervised pre-training. In *Proceedings of the IEEE/CVF Conference on Computer Vision and Pattern Recognition*, pages 13445–13454, 2023. [2](#), [6](#)

[54] Siming Yan, Zhenpei Yang, Haoxiang Li, Chen Song, Li Guan, Hao Kang, Gang Hua, and Qixing Huang. Implicit autoencoder for point-cloud self-supervised representation learning. In *Proceedings of the IEEE/CVF International Conference on Computer Vision*, pages 14530–14542, 2023. [3](#)

[55] Yan Yan, Yuxing Mao, and Bo Li. Second: Sparsely embedded convolutional detection. *Sensors*, 18(10):3337, 2018. [1](#), [2](#)

[56] Bin Yang, Wenjie Luo, and Raquel Urtasun. Pixor: Real-time 3d object detection from point clouds. In *Proceedings of the IEEE conference on Computer Vision and Pattern Recognition*, pages 7652–7660, 2018. [2](#)

[57] Honghui Yang, Tong He, Jiaheng Liu, Hua Chen, Boxi Wu, Binbin Lin, Xiaofei He, and Wanli Ouyang. Gd-mae: generative decoder for mae pre-training on lidar point clouds. In *Proceedings of the IEEE/CVF Conference on Computer Vision and Pattern Recognition*, pages 9403–9414, 2023. [2](#)

[58] Honghui Yang, Sha Zhang, Di Huang, Xiaoyang Wu, Haoyi Zhu, Tong He, Shixiang Tang, Hengshuang Zhao, Qibo Qiu, Binbin Lin, et al. Unipad: A universal pre-training paradigm for autonomous driving. In *Proceedings of the IEEE/CVF Conference on Computer Vision and Pattern Recognition*, pages 15238–15250, 2024. [1](#), [2](#), [3](#), [4](#), [5](#), [7](#), [8](#)

[59] Tianwei Yin, Xingyi Zhou, and Philipp Krahenbuhl. Center-based 3d object detection and tracking. In *Proceedings of the IEEE/CVF conference on computer vision and pattern recognition*, pages 11784–11793, 2021. [1](#), [2](#), [6](#)

[60] Yunpeng Zhang, Jiwen Lu, and Jie Zhou. Objects are different: Flexible monocular 3d object detection. In *Proceedings of the IEEE/CVF Conference on Computer Vision and Pattern Recognition*, pages 3289–3298, 2021. [1](#), [2](#)

[61] Yifan Zhang, Siyu Ren, Junhui Hou, Jinjian Wu, Yixuan Yuan, and Guangming Shi. Self-supervised learning of lidar 3d point clouds via 2d-3d neural calibration. *arXiv preprint arXiv:2401.12452*, 2024. [3](#)

[62] Haoyi Zhu, Honghui Yang, Xiaoyang Wu, Di Huang, Sha Zhang, Xianglong He, Tong He, Hengshuang Zhao, Chunhua Shen, Yu Qiao, et al. Ponderv2: Pave the way for 3d foundataion model with a universal pre-training paradigm. *arXiv preprint arXiv:2310.08586*, 2023. [2](#), [3](#)

001

1. More Implementation Details

002 **Pre-training.** We use a learning rate of 0.00005 with a
003 cosine learning schedule for pre-training and use mask aug-
004 mentation for CLAP with a masking rate of 0.9. All the
005 pre-trainings are conducted on 8-H100 clusters for similar
006 time (~ 45 mins / epoch). As pre-trained image backbones
007 are broadly used for image feature extraction, the imple-
008 mentation of [?] also use a pre-trained image backbone
009 from [?] to initiate their pre-training and the training set
010 for this backbone does not involve any data from NuScenes
011 [?] and Waymo [?]. We adopt this practice for training-
012 from-scratch model and CLAP.

013 **Downstream Training.** We follow the common practice in
014 OpenPCDet [?] and only change the training iterations
015 in order to observe the convergence of train-from-scratch
016 models, which avoids the case that pre-training only accel-
017 erate convergence and make sure that pre-training indeed
018 improve the performance of downstream models. The train-
019 ing epoch is 108 for BEVfusion [?] with 5% of NuScenes
020 [?] training data and 252 for CenterPoint [?] with 1% of
021 Waymo [?] training data.

022 2. More Experiment Results

023 2.1. Semantic Segmentation

024 We fine-tune Cylinder3D [?] for LiDAR semantic seg-
025 mentation on Semantic KITTI dataset [?]. We use mIoU
026 as eval metric. Results are 28.23% for random initializa-
027 tion, 31.88(+3.55)% for UniPAD and 34.28(+6.05)% for
028 CLAP. It can be found that CLAP is able to benefit different
029 tasks and achieves 70% more improvement than UniPAD [?].

031 2.2. Repeated Evaluation

032 We use the same fixed random seed for all experiments in
033 the main paper for reproducibility. As repeated evaluation
034 can further reveal the training robustness, we repeat fine-
035 tunings on NuScenes for 5 times with random initialization,
036 UniPAD and CLAP. Mean and standard deviation of mAP
037 are $48.55 \pm 0.18\%$ (Rand.), $49.66 \pm 0.29\%$ (UniPAD) and
038 $51.16 \pm 0.10\%$ (CLAP). CLAP achieves the best average
039 performance and robustness against random seeds.

040 2.3. Transferring to Other Datasets

041 We conduct further experiments to evaluate the transferring
042 ability of CLAP. Specifically, we select LiDAR-based 3D
043 object detector CenterPoint [?] on Once [?] for the
044 downstream task. A 40-beam LiDAR is utilized in Once
045 [?] to collect 15k labeled training data. We randomly
046 sample 5% and also use all of the labeled training set to
047 train the from-scratch model until convergence is observed.
048 Then we use pre-trained weights by CLAP on NuScenes [?]
049 to initialize the same model and fine-tune it with the same

050 training iterations as the randomly initialized model. Re-
051 sults are shown in Table 1. It can be found that pre-training
052 by CLAP also benefits LiDAR-based 3D object detection,
053 even in a cross-dataset setting. And if we look at the per-
054 formance of “Rand*” and “CLAP*”, CLAP also accelerates
055 the convergence in downstream task.

056 3. Visualization of Prototype Learning

057 We use the model pre-trained by CLAP to infer the 3D fea-
058 tures and assign prototypes to different LiDAR points in the
059 3D space. Then we use different random colors to indicate
060 different prototypes and visualize them in Figure 1. It can
061 be found that the background road plane inside the same
062 frame is generally assigned to the same prototype. And
063 foreground vehicles are assigned to another prototype. This
064 demonstrates that the proposed prototype learning scheme
065 actually learns to represent parts of the scenes with pro-
066 tootypes in an unsupervised manner. However, as our pre-
067 training does not incorporate any label, it can also be found
068 that the prototype assignment has some noise, for example
069 some of the road plane points are assigned to other proto-
070 types.

071 4. Potential Negative Social Impact

072 **Job Displacement.** Automation of tasks that require 3D
073 perception, such as autonomous vehicles or robotics, might
074 lead to job losses in sectors like transportation, warehous-
075 ing, and manufacturing. While automation can create new
076 jobs, the transition period can be challenging for those
077 whose jobs are automated away.

078 **Security Risks.** The deployment of autonomous systems
079 could introduce new vulnerabilities. Any failures in au-
080 tonomous driving or robotics could lead to accidents or be
081 exploited maliciously.

082 **Accessibility and Inequality.** The benefits of advanced
083 3D perception technologies might not be evenly distributed
084 across society. Wealthier regions or organizations may have
085 earlier and better access to these technologies, potentially
086 widening the gap between different socioeconomic groups.

Init.	F.T.	mAP	Vehicle			Pedestrian			Cyclist		
			0-30m	30-50m	50m-	0-30m	30-50m	50m-	0-30m	30-50m	50m-
Rand*	5%	20.48	58.03	25.22	12.98	11.62	9.75	6.97	21.55	6.83	3.11
CLAP*		22.86 +2.38	58.37	26.38	14.07	12.60	9.50	7.88	30.08	10.50	5.39
Rand		46.07	76.71	51.15	31.84	37.53	20.12	9.84	62.00	42.61	24.18
CLAP		46.88 +0.81	76.98	51.64	31.31	38.79	20.60	9.74	63.75	43.21	26.83
Rand*	100%	64.00	86.21	70.20	58.20	57.80	41.18	23.55	75.95	61.45	45.80
CLAP*		64.74 +0.74	88.14	72.59	59.13	57.37	42.24	24.22	77.11	61.91	45.63
Rand		65.03	88.18	74.23	61.75	57.32	38.90	21.96	78.07	64.32	48.16
CLAP		65.56 +0.53	87.97	72.77	62.11	58.33	40.11	21.29	78.63	64.70	47.27

Table 1. Results for transferring experiments on Once [?] dataset. CenterPoint [?] is used as the downstream detector. “Init.” indicates the initialization methods. “F.T.” indicates the number of training samples in fine-tuning stage. Overall mAP and APs for different categories within different ranges are shown in this table. “Rand*” means training the randomly initialized model with the original training iterations in OpenPCDet [?]. “Rand” indicates that we increase the number of training iterations for randomly initialized model until convergence is observed. “CLAP*” indicates that we pre-train the backbones with CLAP on NuScenes [?] and then fine-tune on Once with the original iterations in [?]. “CLAP” uses the same fine-tuning iterations as “Rand”. We use green color to highlight the performance improvement brought by CLAP. All the results are in %.

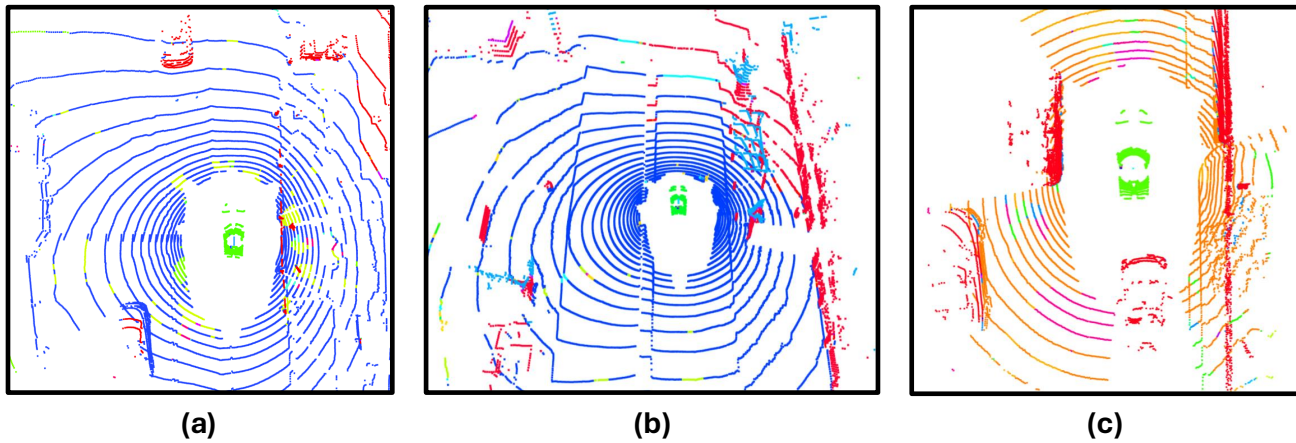


Figure 1. Visualization of the prototype learning results. Different color indicates different prototype assignments.